Energy & Environmental Science

COMMUNICATION

View Article Online
View Journal

Facile synthesis of Li_2S–polypyrrole composite structures for high-performance Li_2S cathodes†

Cite this: DOI: 10.1039/c3ee43395a

Received 12th October 2013
Accepted 29th November 2013

DOI: 10.1039/c3ee43395a

www.rsc.org/ees

Zhi Wei Seh,[a] Haotian Wang,[b] Po-Chun Hsu,[a] Qianfan Zhang,[c] Weiyang Li,[a] Guangyuan Zheng,[d] Hongbin Yao[a] and Yi Cui*[ae]

Li_2S is an attractive prelithiated cathode material with a high theoretical capacity of 1166 mA h g^{-1}, which is far above that of its transition metal oxide/phosphate counterparts. Here, we demonstrate facile, *in situ* synthesis of Li_2S–polypyrrole composites for use as high-performance Li_2S cathodes. The N atoms in polypyrrole were found to possess favorable Li–N interaction with Li_2S, which enables polypyrrole to bind strongly onto and cover the surface of Li_2S to constrain intermediate polysulfides during cycling. Polypyrrole, being a conducting polymer, also helps to facilitate electronic conduction. Using the Li_2S–polypyrrole composites as a cathode material, we demonstrate a high discharge capacity of 785 mA h g^{-1} of Li_2S (~1126 mA h g^{-1} of S) with stable cycling over prolonged 400 charge/discharge cycles.

Broader context

The development of high-capacity cathode materials for use in high-energy rechargeable batteries is important for applications such as vehicle electrification and grid energy storage. Sulfur is a well-known cathode material that is now under intensive study, but further progress is hindered by the need for pairing with a lithium metal anode which is prone to dendrite formation and safety issues. Compared to sulfur, fully lithiated Li_2S represents a more attractive cathode material because it enables pairing with safer, lithium metal-free anodes (such as silicon or tin). However, Li_2S cathodes are plagued with low electronic and ionic conductivity as well as dissolution of intermediate polysulfides into the electrolyte, resulting in fast capacity fading. Herein, we demonstrate the first encapsulation of Li_2S with a conducting polymer, polypyrrole, forming a composite cathode with stable and long-term cycling performance.

Introduction

Energy storage devices based on rechargeable lithium-ion batteries are now widely used in portable electronics and consumer devices today.[1–6] However, the energy density of current lithium-ion batteries remains insufficient for many emerging applications such as vehicle electrification and grid energy storage.[1–6] As a result, much effort has been devoted to the development of alternative high-capacity anode materials (such as silicon and tin),[7,8] but the major limiting factor is still the relatively low capacity of cathodes.[9–29] Li_2S is a promising cathode material with a high theoretical capacity of 1166 mA h g^{-1} based on the electrochemical reaction: $8Li_2S \leftrightarrow S_8 + 16Li$.[30–38] Unlike conventional sulfur cathodes, Li_2S is fully lithiated and can be paired with lithium metal-free anodes (such as silicon and tin), hence obviating dendrite formation and safety concerns associated with metallic lithium.[9–38] Moreover, unlike sulfur which expands 80% during initial lithiation, Li_2S shrinks as it is delithiated initially, generating empty space for subsequent volumetric expansion during lithiation, thus mitigating against structural damage to the electrode.[27,28] However, Li_2S cathodes are known to suffer from low electronic and ionic conductivity as well as dissolution of intermediate lithium polysulfide species (Li_2S_n) into the electrolyte, resulting in fast capacity fading and low Coulombic efficiency.[30–38] To alleviate these problems, the most common strategy is to encapsulate Li_2S with conductive carbon black or mesoporous carbon.[30–35] However, carbon, being non-polar in nature, does not possess favorable binding with highly polar Li_2S, hence preventing carbon from wrapping tightly around Li_2S to help constrain intermediate Li_2S_n species during cycling. As a result, the typical cycle life of Li_2S cathodes demonstrated in the literature has been limited to 100 cycles or less.[30–37]

[a]*Department of Materials Science and Engineering, Stanford University, Stanford, California 94305, USA. E-mail: yicui@stanford.edu*

[b]*Department of Applied Physics, Stanford University, Stanford, California 94305, USA*

[c]*School of Materials Science and Engineering, Beihang University, Beijing 100191, P.R. China*

[d]*Department of Chemical Engineering, Stanford University, Stanford, California 94305, USA*

[e]*Stanford Institute for Materials and Energy Science, SLAC National Accelerator Laboratory, Menlo Park, California 94025, USA*

† Electronic supplementary information (ESI) available: Details of materials synthesis, characterization, *ab initio* simulations, electrochemical measurements, electrolyte testing, Table S1 and Fig. S1–S5. See DOI: 10.1039/c3ee43395a

Herein, we demonstrate, for the first time, the encapsulation of Li_2S with a conducting polymer for use as a high-performance cathode material. In particular, we synthesized a Li_2S–polypyrrole (PPy) composite structure *via* facile, *in situ* polymerization of pyrrole on Li_2S particles. The N atoms in PPy were found to possess favorable Li–N interaction with Li_2S, which enables PPy to bind strongly onto and cover the surface of Li_2S to constrain intermediate Li_2S_n species during cycling. PPy, being a conducting polymer, also helps to facilitate electronic conduction. Using the Li_2S–PPy composites as a cathode material, a high discharge capacity of 785 mA h g^{-1} of Li_2S (~1126 mA h g^{-1} of S) was achieved with stable cycling over prolonged 400 charge/discharge cycles.

Results and discussion

Experimentally, the Li_2S–PPy composites were synthesized *via in situ*, non-aqueous polymerization of pyrrole onto Li_2S particles. Briefly, micron-sized commercial Li_2S particles were first dispersed in anhydrous methyl acetate containing $FeCl_3$ as an oxidant and poly(vinyl acetate) as a stabilizing agent,[39] followed by the addition of pyrrole for overnight polymerization at room temperature (see ESI† for details). Fig. 1a and b show scanning electron microscopy (SEM) images of the Li_2S particles before and after PPy coating, respectively. We can see the formation of multiple PPy nanocolloids (~700 nm) covering the surface of the Li_2S particles, forming a raspberry-like Li_2S–PPy composite structure (Fig. 1b–d). Using energy-dispersive X-ray spectroscopy (EDX), we performed elemental mapping on a representative Li_2S–PPy structure shown in Fig. 1d, which confirms the presence of both sulfur and carbon (Fig. 1e and f; lithium cannot be detected using EDX). The elemental composition of the Li_2S–PPy composites was also studied using EDX analysis, from which the Li_2S content in the composites was determined to be ~86 wt% (see ESI, Table S1† for details).

The Li_2S–PPy composites were further characterized using X-ray diffraction (XRD) and Raman spectroscopy. The XRD pattern of pristine Li_2S in Fig. 2a shows the characteristic diffraction peaks belonging to Li_2S (JCPDS 26-1188; the peak at 22° arises due to the Kapton tape used to protect the samples from moisture in the air; ESI, Fig. S1†). We see that the XRD spectrum of the Li_2S–PPy composites shows only the diffraction peaks of Li_2S but not those of PPy (Fig. 2a), indicating the amorphous nature of PPy. To confirm this, PPy nanocolloids were also prepared in the same way as that of Li_2S–PPy composites except without the Li_2S particles (ESI, Fig. S2†), and their XRD spectrum shows the absence of diffraction peaks (Fig. 2a), thus verifying the amorphous nature of PPy prepared using this method. Upon Raman analysis, we see that the Raman spectrum of pristine Li_2S shows the characteristic T_{2g} phonon mode of Li_2S at 372 cm^{-1} corresponding to Li–S bond vibrations,[40,41] and that of PPy nanocolloids shows the characteristic peaks corresponding to deformation and stretching of the C–H, C=C and N–H bonds in PPy (Fig. 2b).[42] The Raman spectrum of the Li_2S–PPy composites shows both the peaks of Li_2S and PPy, though the intensity of the Li_2S T_{2g} peak is very weak compared to PPy (Fig. 2b). Since Raman spectroscopy is a surface-sensitive technique, this observation indicates that the surface of the Li_2S particles has been largely covered by PPy, which is consistent with the SEM images of the composites in Fig. 1b and d.

To elucidate the interaction between Li_2S and PPy, *ab initio* simulations were performed in the framework of density functional theory (see ESI† for details). The simulation results indicate that the lone pairs on the electronegative N atoms in PPy are capable of binding with Li in Li_2S, forming a

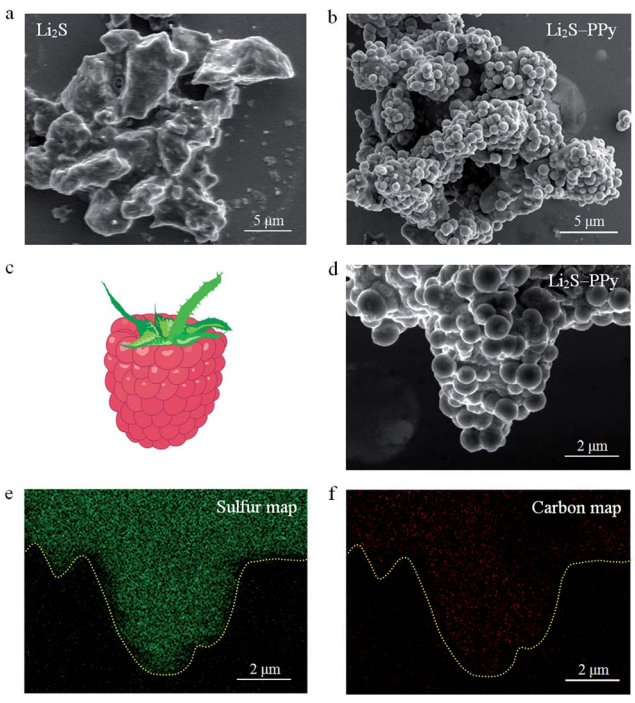

Fig. 1 SEM images of (a) pristine Li_2S particles and (b) as-synthesized Li_2S–PPy composite structures. (c) Schematic of a raspberry and (d) SEM image of a representative Li_2S–PPy raspberry-like composite together with the corresponding elemental maps for (e) sulfur and (f) carbon.

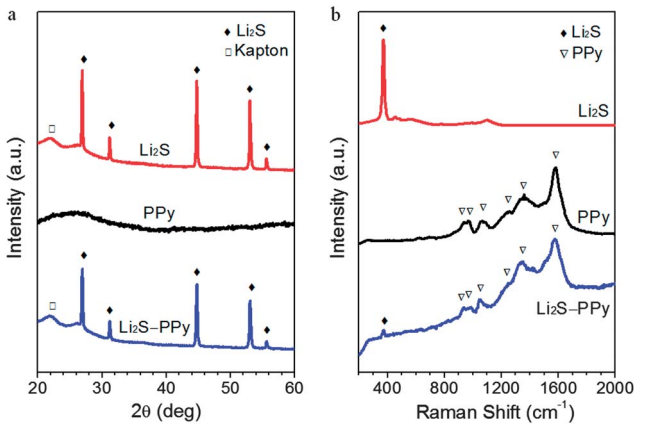

Fig. 2 (a) XRD patterns and (b) Raman spectra of pristine Li_2S, PPy nanocolloids and Li_2S–PPy composites. The XRD peak at 22° arises due to the Kapton tape used to protect the Li_2S-containing samples from moisture in the air.

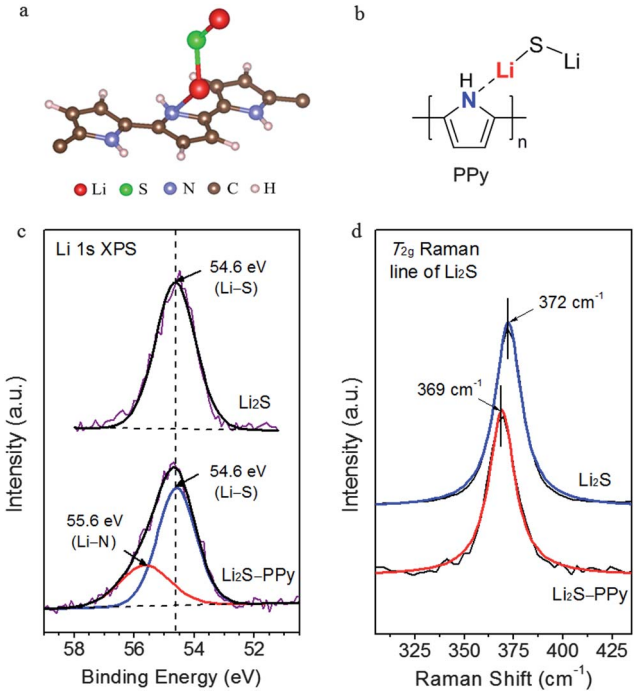

Fig. 3 (a) *Ab initio* simulations and (b) schematic showing the most stable binding configuration of Li_2S with PPy corresponding to Li–N interaction. (c) High-resolution XPS spectra of the Li 1s peak and (d) Raman spectra of the T_{2g} Raman peak of Li_2S in the pristine Li_2S and Li_2S–PPy composites together with their respective fitted peaks.

coordination-like interaction (Fig. 3a and b). The binding energy between Li_2S and PPy was calculated to be 0.50 eV. The results also show similar Li–N interaction between PPy and Li–S· species, the relevant end groups in lithium polysulfides (Li–S–S_{n-2}–S–Li; Li_2S_n in short),[38] which would enable PPy to constrain these polysulfide species during cycling (ESI, Fig. S3†). To investigate the Li–N interaction between Li_2S and PPy in the composite structure, we performed high-resolution X-ray photoelectron spectroscopy (XPS). To prevent moisture contamination of Li_2S, special precautions were taken during characterization (see ESI† for details). The as-obtained Li 1s XPS spectrum of pristine Li_2S can be fitted with a single peak with a binding energy of 54.6 eV (Fig. 3c) corresponding to Li in the Li–S bond.[43] In comparison, the Li 1s spectrum of the Li_2S–PPy composites shows asymmetric broadening towards higher binding energy (Fig. 3c), indicating a change in chemical environment experienced by Li. A good fit of this spectrum was obtained using 2 peaks at 54.6 eV and 55.6 eV, which can be attributed to Li–S and Li–N interactions respectively (Fig. 3c), in accordance with tabulated values.[43] The appearance of this additional Li–N peak, which is absent in the pristine Li_2S sample, is indicative of Li–N interaction between Li_2S and PPy in the composite structure, consistent with the *ab initio* simulation results described above.

To provide further evidence in support of the interaction between Li_2S and PPy, we performed Raman spectroscopy and analyzed the T_{2g} Raman peak of Li_2S in the pristine Li_2S and Li_2S–PPy composite samples. The T_{2g} Raman peak of pristine Li_2S was measured at 372 cm^{-1} (Fig. 3d), in accordance with values in the literature.[40,41] Interestingly, we see a red-shift in the Raman peak position from 372 cm^{-1} in pristine Li_2S to 369 cm^{-1} in the Li_2S–PPy composites (Fig. 3d). Since the T_{2g} phonon mode in Li_2S is ascribed to Li–S bond vibrations,[40,41] a red-shift indicates a decrease in the force constant and slight weakening of the Li–S bond in the Li_2S–PPy composites.[44,45] This can be attributed to the electronegative N atoms in PPy interacting with Li in Li_2S, causing the electron density along the Li–S bond in Li_2S to be diminished and the bond to be weakened, as indicated by Raman spectroscopy.

To evaluate the electrochemical performance of the Li_2S–PPy composites, 2032-type coin cells were assembled. The working electrodes were prepared by mixing the Li_2S–PPy composites with carbon black and binder (60 : 35 : 5 by weight) in *N*-methyl-2-pyrrolidinone to form a slurry, which was then coated onto aluminum foil and dried in a glove box. 2032-Type coin cells were then assembled with lithium foil as the counter electrode. The electrolyte used was lithium bis(trifluoromethanesulfonyl)-imide in 1 : 1 v/v 1,2-dimethoxyethane and 1,3-dioxolane with $LiNO_3$ additive. The Li_2S–PPy composite cathodes were first activated at C/20 (1 C = 1166 mA g^{-1}) by charging to a high cutoff voltage of 3.8 V *vs.* Li^+/Li to overcome the initial potential barrier associated with micron-sized Li_2S particles (ESI, Fig. S4†),[33] followed by discharge to 1.8 V. Galvanostatic cycling was then carried out from 1.8 to 2.6 V *vs.* Li^+/Li. The typical mass loading of Li_2S was ~1 mg cm^{-2} and specific capacity values were calculated based on the mass of Li_2S.

The Li_2S–PPy composite cathodes exhibited stable cycling performance at 0.2 C with a high initial capacity of 785 mA h g^{-1} of Li_2S (theoretical capacity 1166 mA h g^{-1}) as displayed in Fig. 4a. Relative to the initial cycle, the capacity retention values achieved at the end of 50, 100 and 200 cycles were 91%, 91% and 84% respectively. Even after prolonged cycling over 400 charge/discharge cycles, the cells retained 73% of their initial capacity, which corresponds to a small average capacity decay of 0.068% per cycle (Fig. 4a). The average Coulombic efficiency over 400 cycles was calculated to be 95% (Fig. 4a). For comparison, cells were also assembled using pristine Li_2S cathodes, which exhibited faster capacity decay under identical testing conditions (Fig. 4b). The capacity retention of the pristine Li_2S cathodes was only 63% after 100 cycles (compared to 91% for Li_2S–PPy composites), indicating a greater degree of polysulfide dissolution into the electrolyte in the former case. This is supported by testing of the electrolyte for sulfur content using inductively coupled plasma-optical emission spectroscopy (ICP-OES) at various intermediate stages during a discharge/charge cycle (see ESI† for details).[38] Points 1 to 10 in Fig. 4c correspond to various depths of discharge (DOD) and states of charge (SOC) during cycling. The ICP-OES results show a consistently lower percentage loss of sulfur into the electrolyte at various stages of cycling for the Li_2S–PPy composites compared to pristine Li_2S cathodes (Fig. 4d and e). For instance, at point 3 corresponding to 25% DOD, a maximum of 34% of the total sulfur mass on the electrode was found to be dissolved in the electrolyte for the Li_2S–PPy composites, compared to 86% in the case of pristine Li_2S cathodes (Fig. 4d). Similarly, at point

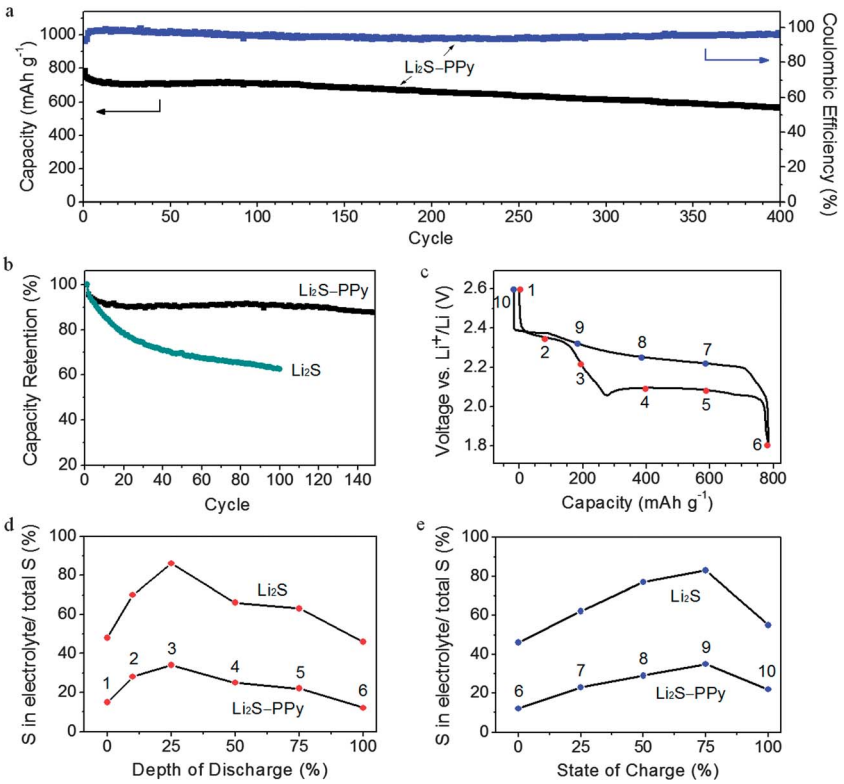

Fig. 4 (a) Specific capacity and Coulombic efficiency of Li_2S–PPy composite cathodes upon prolonged cycling over 400 cycles at 0.2 C. (b) Capacity retention of Li_2S–PPy composite cathodes cycled at 0.2 C in comparison with pristine Li_2S cathodes. (c) Typical discharge and charge voltage profile showing various depths of discharge and states of charge (points 1 to 10) and (d and e) the corresponding percentage of sulfur measured in the electrolyte relative to the total sulfur mass on the electrode at these various points for Li_2S–PPy composite and pristine Li_2S cathodes. Specific capacity values were calculated based on the mass of Li_2S.

9 corresponding to 75% SOC, 35% dissolution of the total sulfur mass into the electrolyte was measured for the Li_2S–PPy composites, compared to 83% in the case of pristine Li_2S cathodes (Fig. 4e). This indicates that the presence of PPy covering the surface of Li_2S (through strong Li–N interaction) helps to constrain intermediate Li_2S_n species to reduce their loss into the electrolyte, resulting in more stable cycling performance.

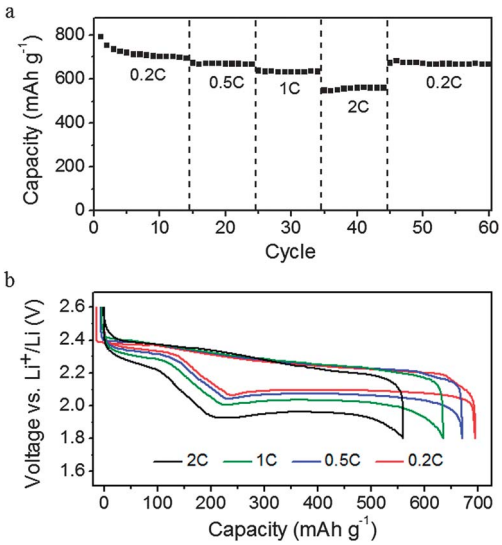

Fig. 5 (a) Specific capacity and (b) voltage profiles of Li_2S–PPy composite cathodes cycled at various C-rates from 0.2 C to 2 C. Specific capacity values were calculated based on the mass of Li_2S.

Next, the Li_2S–PPy composite cathodes were subject to cycling at various C-rates to evaluate their electrode kinetics and stability (Fig. 5a and b). When the C-rate was increased successively from 0.2 to 0.5 to 1 to 2 C, the cells delivered high stabilized capacities of 695, 670, 635 and 560 mA h g^{-1} of Li_2S respectively (Fig. 5a). The capacities achieved at 0.5, 1 and 2 C correspond to 96%, 91% and 81% of the capacity that was attained at 0.2 C, indicating good reaction kinetics in the cathodes. When the C-rate was switched abruptly from 2 C back to 0.2 C again, 98% of the original capacity was recovered (Fig. 5a), indicating robustness and stability of the cathode material. Finally, the morphology of the Li_2S–PPy composite cathodes was also examined after 50 cycles at 0.2 C. At the end of 50 cycles, the voltage was maintained at 1.8 V *vs.* Li^+/Li for over 20 h and the cell was disassembled in the discharged state. We see that Li_2S–PPy composites largely retain their original morphology after cycling, with PPy nanocolloids still covering the surface of the Li_2S particles (ESI, Fig. S5†).

Conclusion

We have demonstrated the facile synthesis of Li_2S–PPy composite cathodes, in which favorable Li–N interaction

enables strong binding of PPy onto the surface of Li_2S to help constrain intermediate Li_2S_n species during cycling. Additional work is ongoing to achieve a more complete encapsulation of Li_2S with other conducting polymers to further mitigate against polysulfide dissolution into the electrolyte. This work provides new avenues for the future development of strongly bound conducting polymer coatings for Li_2S cathodes to achieve good cycling stability and long cycle life.

Acknowledgements

This work was supported as part of the Joint Center for Energy Storage Research (JCESR), an Energy Innovation Hub funded by the U.S. Department of Energy, Office of Science, Basic Energy Sciences. Z.W.S. and G.Z. acknowledge the support of an A*STAR National Science Scholarship.

References

1 B. Kang and G. Ceder, *Nature*, 2009, **458**, 190–193.
2 Y.-M. Chiang, *Science*, 2010, **330**, 1485–1486.
3 M. S. Whittingham, *Chem. Rev.*, 2004, **104**, 4271–4301.
4 J. B. Goodenough and K.-S. Park, *J. Am. Chem. Soc.*, 2013, **135**, 1167–1176.
5 Y. Zhao, B. Liu, L. Pan and G. Yu, *Energy Environ. Sci.*, 2013, **6**, 2856–2870.
6 B. Scrosati, J. Hassoun and Y. K. Sun, *Energy Environ. Sci.*, 2011, **4**, 3287–3295.
7 L. W. Ji, Z. Lin, M. Alcoutlabi and X. W. Zhang, *Energy Environ. Sci.*, 2011, **4**, 2682–2699.
8 H. Wu and Y. Cui, *Nano Today*, 2012, **7**, 414–429.
9 B. Zhang, X. Qin, G. R. Li and X. P. Gao, *Energy Environ. Sci.*, 2010, **3**, 1531–1537.
10 L. Ji, M. Rao, S. Aloni, L. Wang, E. J. Cairns and Y. Zhang, *Energy Environ. Sci.*, 2011, **4**, 5053–5059.
11 T. H. Hwang, D. S. Jung, J.-S. Kim, B. G. Kim and J. W. Choi, *Nano Lett.*, 2013, **13**, 4532–4538.
12 H. Yamin, A. Gorenshtein, J. Penciner, Y. Sternberg and E. Peled, *J. Electrochem. Soc.*, 1988, **135**, 1045–1048.
13 P. G. Bruce, S. A. Freunberger, L. J. Hardwick and J.-M. Tarascon, *Nat. Mater.*, 2012, **11**, 19–29.
14 X. Ji, K. T. Lee and L. F. Nazar, *Nat. Mater.*, 2009, **8**, 500–506.
15 X. Ji, S. Evers, R. Black and L. F. Nazar, *Nat. Commun.*, 2011, **2**, 325.
16 N. Jayaprakash, J. Shen, S. S. Moganty, A. Corona and L. A. Archer, *Angew. Chem., Int. Ed.*, 2011, **50**, 5904–5908.
17 R. Elazari, G. Salitra, A. Garsuch, A. Panchenko and D. Aurbach, *Adv. Mater.*, 2011, **23**, 5641–5644.
18 S. Xin, L. Gu, N.-H. Zhao, Y.-X. Yin, L.-J. Zhou, Y.-G. Guo and L.-J. Wan, *J. Am. Chem. Soc.*, 2012, **134**, 18510–18513.
19 Z. Lin, Z. Liu, W. Fu, N. J. Dudney and C. Liang, *Angew. Chem., Int. Ed.*, 2013, **52**, 7460–7463.
20 J. L. Wang, J. Yang, J. Y. Xie and N. X. Xu, *Adv. Mater.*, 2002, **14**, 963–965.
21 M. Sun, S. Zhang, T. Jiang, L. Zhang and J. Yu, *Electrochem. Commun.*, 2008, **10**, 1819–1822.
22 L. Xiao, Y. Cao, J. Xiao, B. Schwenzer, M. H. Engelhard, L. V. Saraf, Z. Nie, G. J. Exarhos and J. Liu, *Adv. Mater.*, 2012, **24**, 1176–1181.
23 Y. Cao, X. Li, I. A. Aksay, J. Lemmon, Z. Nie, Z. Yang and J. Liu, *Phys. Chem. Chem. Phys.*, 2011, **13**, 7660–7665.
24 Y. Fu and A. Manthiram, *J. Phys. Chem. C*, 2012, **116**, 8910–8915.
25 Y.-S. Su and A. Manthiram, *Nat. Commun.*, 2012, **3**, 1166.
26 L. Suo, Y.-S. Hu, H. Li, M. Armand and L. Chen, *Nat. Commun.*, 2013, **4**, 1481.
27 Z. W. Seh, W. Li, J. J. Cha, G. Zheng, Y. Yang, M. T. McDowell, P.-C. Hsu and Y. Cui, *Nat. Commun.*, 2013, **4**, 1331.
28 W. Li, G. Zheng, Y. Yang, Z. W. Seh, N. Liu and Y. Cui, *Proc. Natl. Acad. Sci. U. S. A.*, 2013, **110**, 7148–7153.
29 G. Zheng, Q. Zhang, J. J. Cha, Y. Yang, W. Li, Z. W. Seh and Y. Cui, *Nano Lett.*, 2013, **13**, 1265–1270.
30 J. Hassoun and B. Scrosati, *Angew. Chem., Int. Ed.*, 2010, **49**, 2371–2374.
31 M. Nagao, A. Hayashi and M. Tatsumisago, *J. Mater. Chem.*, 2012, **22**, 10015–10020.
32 Y. Yang, M. T. McDowell, A. Jackson, J. J. Cha, S. S. Hong and Y. Cui, *Nano Lett.*, 2010, **10**, 1486–1491.
33 Y. Yang, G. Zheng, S. Misra, J. Nelson, M. F. Toney and Y. Cui, *J. Am. Chem. Soc.*, 2012, **134**, 15387–15394.
34 K. Cai, M.-K. Song, E. J. Cairns and Y. Zhang, *Nano Lett.*, 2012, **12**, 6474–6479.
35 J. Guo, Z. Yang, Y. Yu, H. D. Abruna and L. A. Archer, *J. Am. Chem. Soc.*, 2013, **135**, 763–767.
36 Z. Lin, Z. Liu, N. J. Dudney and C. Liang, *ACS Nano*, 2013, **7**, 2829–2833.
37 Y. Fu, Y.-S. Su and A. Manthiram, *Adv. Energy Mater.*, 2013, DOI: 10.1002/aenm.201300655.
38 Z. W. Seh, Q. Zhang, W. Li, G. Zheng, H. Yao and Y. Cui, *Chem. Sci.*, 2013, **4**, 3673–3677.
39 S. P. Armes and M. Aldissi, *Synth. Met.*, 1990, **37**, 137–144.
40 B. Bertheville, H. Bill and H. Hagemann, *J. Phys.: Condens. Matter*, 1998, **10**, 2155–2169.
41 A. Grzechnik, A. Vegas, K. Syassen, I. Loa, M. Hanfland and M. Jansen, *J. Solid State Chem.*, 2000, **154**, 603–611.
42 Y. Furukawa, S. Tazawa, Y. Fujii and I. Harada, *Synth. Met.*, 1988, **24**, 329–341.
43 J. F. Moulder and J. Chastain, *Handbook of X-ray photoelectron spectroscopy: a reference book of standard spectra for identification and interpretation of XPS data*, Physical Electronics Division, Perkin-Elmer Corp, 1995.
44 C. Q. Sun, L. K. Pan, C. M. Li and S. Li, *Phys. Rev. B: Condens. Matter Mater. Phys.*, 2005, **72**, 134301.
45 M. X. Gu, L. K. Pan, B. K. Tay and C. Q. Sun, *J. Raman Spectrosc.*, 2007, **38**, 780–788.